DOI: 10.1002/ejoc.201300443

Synthesis, Molecular and Photovoltaic Properties of an Indolo[3,2-*b*]indole-Based Acceptor–Donor–Acceptor Small Molecule

Yu-Ying Lai,[a] Jyun-Ming Yeh,[a] Che-En Tsai,[a] and Yen-Ju Cheng*[a]

Keywords: Nitrogen heterocycles / Donor–acceptor systems / Conjugation / Semiconductors / Photophysics

Indolo[3,2-*b*]indole, containing two fused indole units, is an unexplored but promising electron-rich molecule for constructing donor–acceptor materials due to its planar, symmetric, and extended conjugated structure. We have successfully developed a new synthetic pathway to prepare 2,7-diboronic ester-indolo[3,2-*b*]indole, which was then reacted with dithienodiketopyrrolo-pyrrole acceptor to afford a new acceptor–donor–acceptor (A–D–A) conjugated molecule, 2,7-bis(dithienodiketopyrrolo-pyrrole)indolo[3,2-*b*]indole (2,7-DPPIIDPP). **II** is used to stand for indolo[3,2-*b*]indole in order to emphasize that this compound is constructed from two indole units. The A–D–A linkage through the 2,7-positions of **II** not only preserves the phenylene units in the *para*-conjugation but also renders stronger electron-donating strength. This material exhibited good thermal stability, high crystallinity, and broad UV/Vis absorption. The solution-processed bulk heterojunction device using the configuration of ITO/PEDOT:PSS/2,7-DPPIIDPP:$PC_{71}BM$/Ca/Al exhibited a V_{oc} of 0.72 V, a J_{sc} of 6.88 mA/cm^2, and an FF of 49.6 %, leading to a power conversion efficiency (PCE) of 2.45 %.

Introduction

Research on organic p-type (donor) and n-type (acceptor) semiconductors in the field of bulk-heterojuction (BHJ) solar cells has developed rapidly in recent years.[1] Fullerene derivatives, such as phenyl-C_{61}-butyric acid methyl ester ($PC_{61}BM$), have been regarded as irreplaceable n-type materials for high-performance BHJ solar cells. Considerable research effort is thus been directed toward the development of p-type conjugated molecules, polymers especially. In this context, studies of small molecules are relatively scarce.[2] However, in comparison to polymeric counterparts, small molecules in principle have many advantages, including monodispersity, well-defined structures, no end group contamination, simple purification, more effective intermolecular π–π stacking, and better batch-to-batch reproducibility. Consequently, BHJ solar cells utilizing small molecule p-type materials continue to receive growing attention.[2] The strategy of integrating an electron-rich molecule (donor) with an electron-deficient molecule (acceptor) has been demonstrated to be effective in producing low band-gap conjugated molecules.[3] Carbazole, in which a central pyrrole ring is embedded between two benzene rings, is one of the most classical electron donors for the construction of donor-acceptor conjugated polymers due to its good hole-transportation properties and the ability to induce intramolecular charge transfer (ICT) upon photoexcitation.[4] It was therefore considered promising to further develop a new class of elongated and coplanar conjugated systems comprising multifused benzene and pyrrole components. One molecule belonging to this category is the pentacyclic indolo[3,2-*b*]carbazole, which has been introduced to D–A-conjugated copolymers showing decent photovoltaic performance.[5] On the other hand, indolo[3,2-*b*]indole (**II**), in which the central pyrrolopyrrole is fused with two external benzene rings, emerges as an appealing synthetic target due to its many superior molecular properties (Scheme 1). With one more embedded pyrrole moiety than carbazole, indolo[3,2-*b*]indole has more extended conjugation and stronger donating strength, which should result in efficient ICT transition and thereby better light-harvesting. Furthermore, unlike carbazole, with the $C2_v$ symmetry, **II** is a $C2_h$ symmetrical molecule. Pei and co-workers have demonstrated that a $C2_h$ centro-symmetric donor unit can facilitate intermolecular π–π stacking, whereas a $C2_v$ axis-symmetric donor unit has a weaker effect on intermolecular interactions.[6] Therefore, centro-symmetric **II**-based D–A molecules would align in higher order in the solid state, leading to improvements in the hole-transporting properties of the corresponding materials. Furthermore, planar conjugated molecules usually suffer from poor solubility, which hinders solution processability. Two aliphatic chains can be introduced to the nitrogen atoms in **II** to enhance the solubility of the highly planar D–A conjugated molecule. We anticipate that the nitrogen-containing small molecule **II** may not only inherit the intrinsic advantages of carbazole but should also exhibit very interesting optical, electronic, and morphological properties. Herein, we report a new synthetic pathway leading to the preparation of 2,7-diboronic

[a] Department of Applied Chemistry, National Chiao Tung University,
1001 Ta Hseuh Road, Hsin-Chu 30010, Taiwan
E-mail: yjcheng@mail.nctu.edu.tw

Supporting information for this article is available on the WWW under http://dx.doi.org/10.1002/ejoc.201300443.

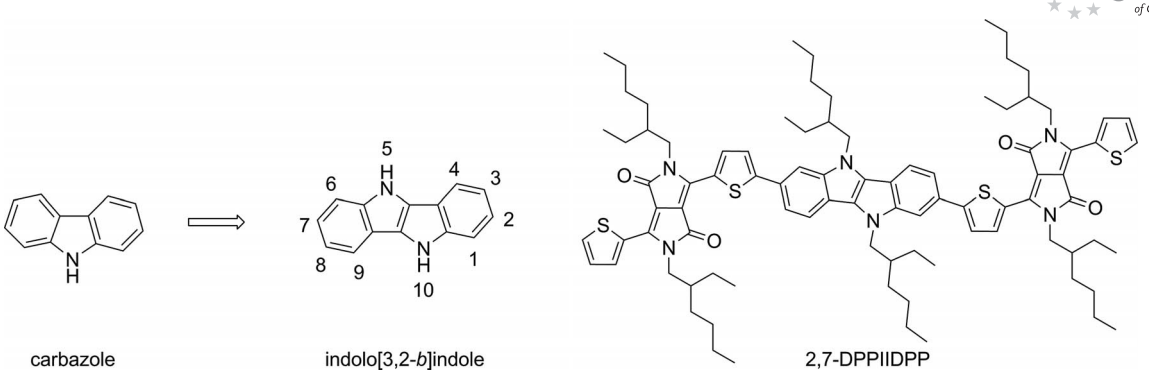

Scheme 1. Structures of carbazole, indolo[3,2-*b*]indole (**II**), and 2,7-DPPIIDPP. Numerical locants of indolo[3,2-*b*]indole are listed for clarity in nomenclature.

ester indolo[3,2-*b*]indole. Electron-rich monomer **II** was coupled with two electron-deficient dithienodiketopyrrolopyrrole (DPP)[7] moieties to yield 2,7-bis(dithienodiketopyrrolo-pyrrole)indolo[3,2-*b*]indole (2,7-DPPIIDPP) with an acceptor–donor–acceptor (A–D–A) arrangement (Scheme 1). Its thermal, optical, and electrochemical properties and X-ray diffraction have been characterized and theoretical calculations were performed. Photovoltaic devices based on this solution-processed 2,7-DPPIIDPP small molecule have delivered good performance.

Results and Discussion

Synthesis

Attachment of **II** with two dithienodiketopyrrolo-pyrrole (DPP) units can be carried out either through the 3,8-positions or 2,7-positions of **II** to produce DPPIIDPP conjugated molecules. The position of the linkage may play an important role in determining the electronic and steric properties of the resulting DPPIIDPP molecules. 2,7-Exten-

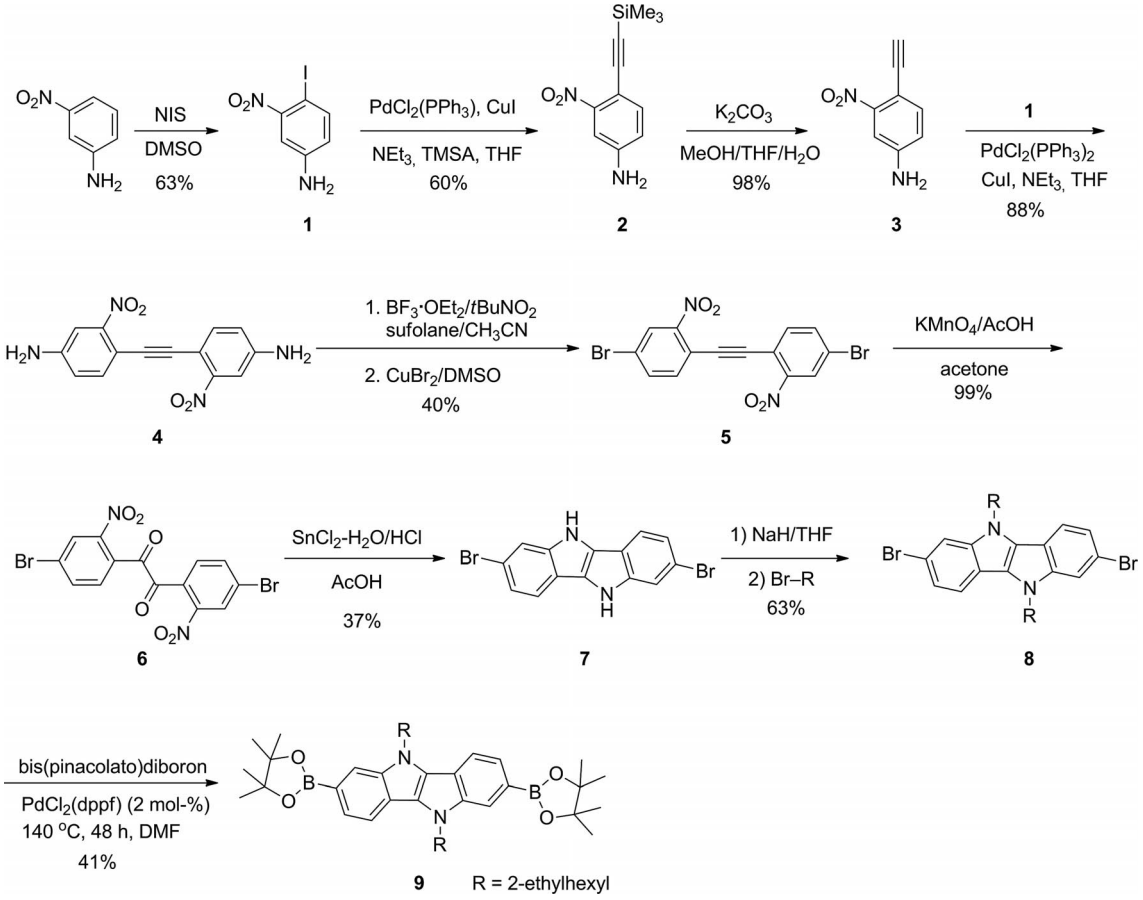

Scheme 2. Synthesis of the 2,7-diboronic ester of the indolo[3,2-*b*]indole unit **II** .

sion can maintain *para*-linkage of the phenylene, resulting in a more effective conjugation length. On the other hand, 3,8-extension leads to the nitrogen atoms *para* to the acceptor moieties, which may induce stronger D–A interaction. The disparity between the electronic and steric properties derived from the two different connecting modes (2,7- vs. 3,8-positions of **II**) can therefore be investigated. The synthetic route via 2,7-dibromoindolo[3,2-*b*]indole is depicted in Scheme 2. Regioselective iodination of 3-nitroaniline with *N*-iodosuccinimide (NIS) in dimethyl sulfoxide (DMSO) yielded **1**,[8] which then underwent Sonogashira reaction with (trimethylsilyl)acetylene to afford **2**. Desilylation of **2** by treatment with potassium carbonate furnished **3**. Sonogashira reaction of **1** with **3** led to the formation of **4**. Treatment of the latter with $BF_3{\cdot}OEt_2/t$BuNO$_2$ to form the diazonium salt followed by reaction with $CuBr_2$ yielded the brominated compound **5**. Oxidation of the acetylene group of **5** by $KMnO_4$/AcOH gave **6**. Reduction of the nitro groups of **6** by $SnCl_2$, followed by acid-prompted intramolecular cyclization furnished **7**. *N*-Alkylation of **7** by using 2-ethylhexyl bromide in the presence of sodium hydride in tetrahydrofuran (THF) afforded 2,7-dibromo-5,10-diethylhexylindolo[3,2-*b*]indole (**8**), which was treated with bis(pinacolato)diboron in the presence of [$PdCl_2$(dppf)] [dppf = 1,1′-bis(diphenylphosphino)ferrocene] in *N*,*N*-dimethylformamide (DMF) to give 2,7-diboronic ester-indolo[3,2-*b*]indole (**9**).

Bromination of indolo[3,2-*b*]indole is an intriguing chemistry. Bromination at the 3,8-positions of indolo[3,2-*b*]-indole seems to be reasonable according to the *para*-directing effect of the nitrogen atom. However, the regioselectivity of direct bromination of **II** is ambiguous because both 3,8-dibromo- and 2,7-dibromo-indolo[3,2-*b*]indole have been reported to take place under similar conditions.[9] To clarify this controversy, we re-examined this reaction (Scheme 3). By comparing the ^{1}H NMR spectra of compound **8** and the product of the direct bromination, it can be concluded that bromination of indolo[3,2-*b*]indole occurs at the 2,7-positions rather than the 3,8-positions. This result also implies that the 2,7-positions of indolo[3,2-*b*]-indole actually have stronger nucleophilicity than the 3,8-positions, which can be rationalized by analyzing the resonance structures of **II**. As illustrated in Scheme 4, the lone pair electrons on the nitrogen can delocalize into the phenyl ring through the central olefin in the pyrrolopyrrole ring, pushing the π-electrons on the 2- or 7-positions. Consequently, electrophilic aromatic substitution of **II** with bromine selectively occurs at the 2,7-positions. Considering that 2,7-linkage can preserve the phenylene units in the *para*-conjugation, and 2,7-positions are actually the stronger electron-donating sites, we thus focus on the syn-

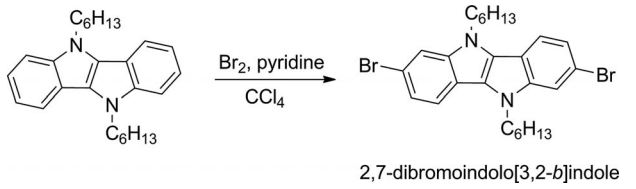

Scheme 3. Bromination of *N*-alkyl-substituted indolo[3,2-*b*]indole by Br_2 and pyridine in CCl_4.

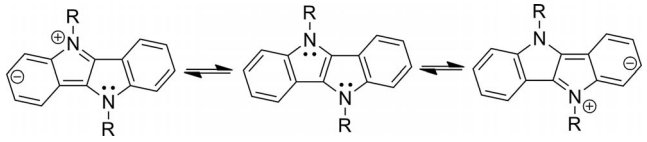

Scheme 4. Resonance structures of indolo[3,2-*b*]indole.

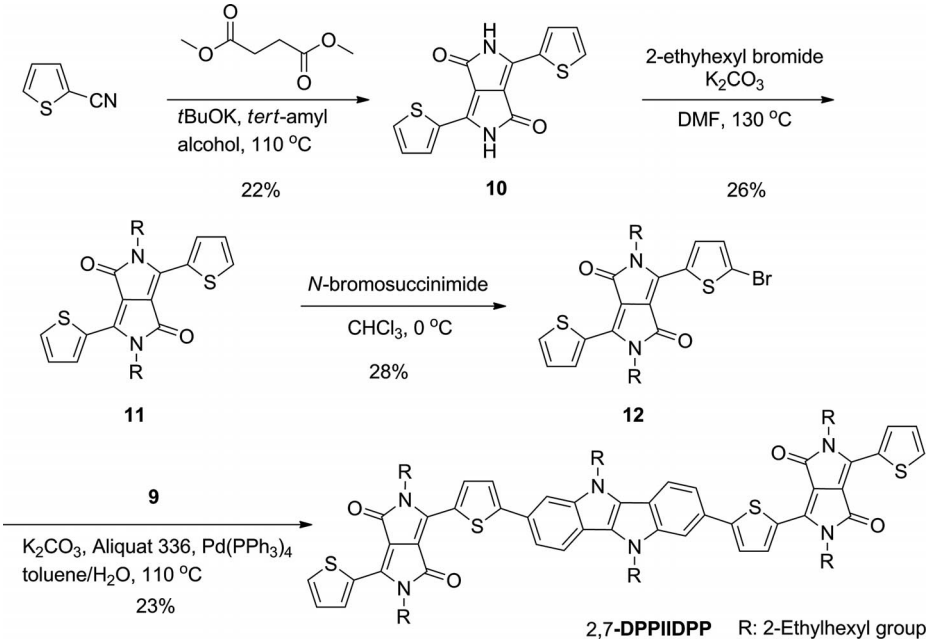

Scheme 5. Synthesis of the DPP unit and 2,7-DPPIIDPP.

thesis of 2,7-substituted **II** monomer and its corresponding acceptor-donor-acceptor small molecule, 2,7-DPPIIDPP.

The synthesis of DPP is described in Scheme 5. Tandem aldol reactions between dimethyl succinate and thiophene-2-carbonitrile accompanied by intramolecular cyclization led to the formation of **10**, which was then alkylated by using 2-ethylhexyl bromide in the presence of potassium carbonate to give **11**. Monobromination of **11** was achieved by using *N*-bromosuccinimide (NBS; 1 equiv.) in chloroform to furnish **12**. The desired product, 2,7-DPPIIDPP, was then successfully synthesized from **9** and **12** through the palladium-catalyzed Suzuki coupling reaction (Scheme 5).

Physical Properties

The thermal properties of 2,7-DPPIIDPP were analyzed by thermogravimetric analysis (TGA). The decomposition temperature (T_d) obtained by TGA was 386 °C, suggesting its thermal stability is sufficient for organic-solar-cell (OSC) applications (Figure 1).

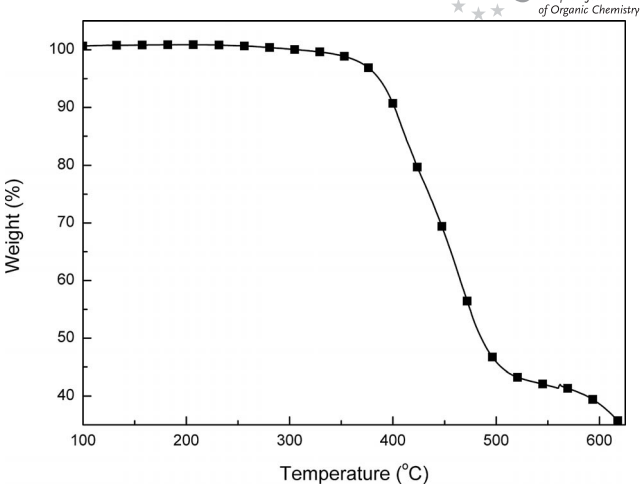

Figure 1. Thermogravimetric analysis (TGA) of 2,7-DPPIIDPP.

Table 1. XRD data of 2,7-DPPIIDPP.

2θ [rad]	d-Spacing [Å]
5.46	16.20
7.60	11.71
11.37	7.78
18.38	4.83

X-ray diffraction (XRD) analysis was employed to examine the morphology of the thin film that was prepared by spin-coating a $CHCl_3$ solution of 2,7-DPPIIDPP on a glass substrate. The XRD patterns are illustrated in Figure 2 and the key d-spacing values are summarized in Table 1. The 2,7-DPPIIDPP film exhibited a strong diffraction peak at 2θ = 5.46°, corresponding to a d-spacing value of 16.20 Å and diffraction peaks at 2θ = 7.60°, 11.37°, and 18.38° were also observed, suggesting an organized assembly and crystallinity of this π-conjugated molecule in the solid state. The crystallinity of this material is highly associated with its coplanar structure (the optimized geometry of 2,7-DPPIIDPP is depicted in Figure 5 below).

Cyclic voltammetry (CV) was employed to study the electrochemical properties. The HOMO and LUMO levels of 2,7-DPPIIDPP were estimated to be –5.14 and –3.47 eV, respectively, with the corresponding band gap being 1.67 eV.

The absorption spectra of 2,7-DPPIIDPP are shown in Figure 3 and its λ_{max} values are listed in Table 2. It exhibits two distinct bands in the absorption spectrum in the $CHCl_3$ solution. One band at the shorter wavelength region results from localized π–π* transitions and the second band at longer wavelength is attributed to intramolecular charge transfer (see below for a detailed assignment of the absorption bands). Compared with the solution state, the thin-film spectrum exhibited bathochromic shifts and broadening of

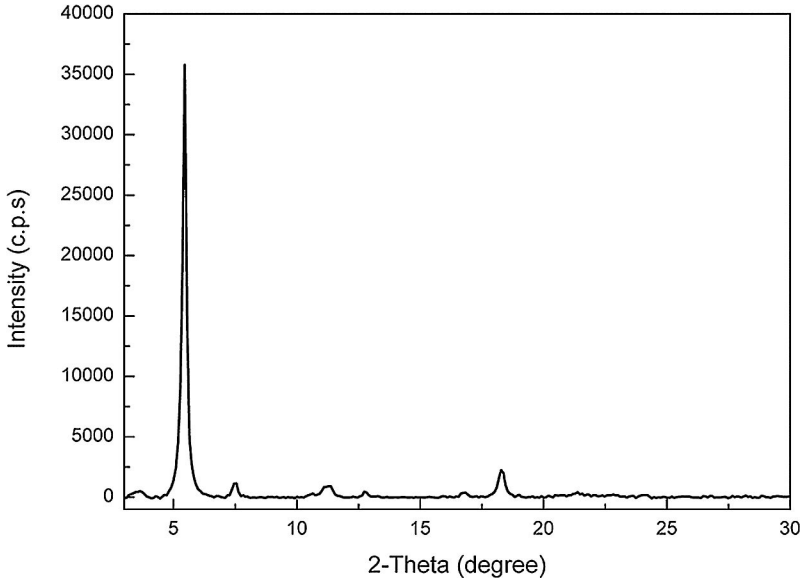

Figure 2. 1-Dimension X-ray diffraction patterns of 2,7-DPPIIDPP.

Table 2. Calculated[a] HOMO/LUMO energy, excitation energy, oscillator strength, and configurations (with large CI coefficients) of the excited state of 2,7-DPPIIDPP.

HOMO [eV][e]	LUMO [eV][e]	Excitation energy [nm] $\lambda_{max,exp}$[b]	$\lambda_{max,exp}$[c]	λ_{calc}	Oscillator strength	Symmetry	Configuration[d]
–4.98 (–5.14)	–2.86 (–3.47)	615	625	673	2.20826	Singlet-A	**H→L**
		415	401	424	0.3767	Singlet-A′′	**H→L+2**
							H–3→L
							H–1→L+3

[a] TD-B3LYP/6-311G(d,p), PCM = $CHCl_3$. [b] Experimental values were measured for non-simplified 2,7-DPPIIDPP in the thin film. [c] Experimental values were measured for non-simplified 2,7-DPPIIDPP in $CHCl_3$ solution. [d] Configurations with largest coefficients in the CI expansion of each state are highlighted in boldface. [e] Experimental values obtained by cyclic voltammetry are given in parentheses.

the π–π* and ICT bands with a shoulder, suggesting that 2,7-DPPIIDPP has stronger intermolecular aggregation in the solid state. Moreover, 2,7-DPPIIDPP possesses a broad absorption coverage ranging from 300 to 800 nm in the solid state, indicating that the electron-donating unit **II** has strong electronic interaction with the electron-deficient DPP units through its 2,7-linkage.

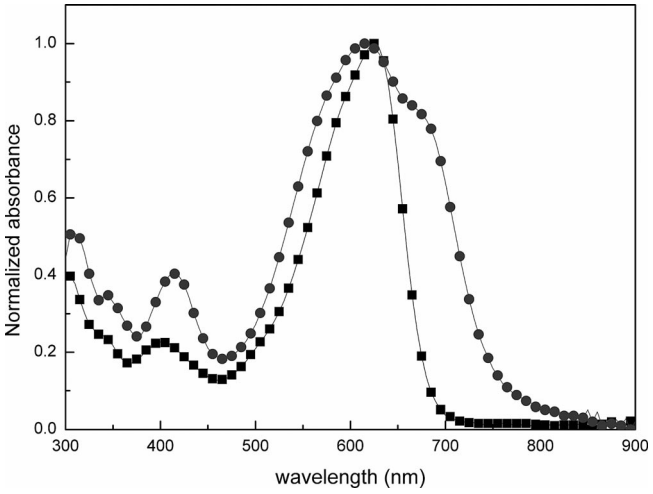

Figure 3. Normalized absorption spectra of 2,7-DPPIIDPP in chloroform solution (squares) and the solid state (circles).

Theoretical Calculations

DFT calculations were carried out with the Gaussian 09 suite at the B3LYP/6-311G (d,p) level of theory to investigate the chemical reactivity of **II**; the calculations were simplified by replacing the hexyl substituents with methyl groups. Chemical reactivity of a molecule is highly associated to its frontier orbitals, i.e., HOMO and LUMO,[10] which can provide useful information on the regioselectivity of **II** for electrophilic aromatic substitution. Figure 4 illustrates the calculated HOMO of **II**, in which the carbon atoms at the 2,7-positions possess much higher electron density than those at the 3,8-positions, implying that the 2,7-positions of indolo[3,2-*b*]indole have stronger nucleophilicity than the 3,8-positions. The result is consistent with the experimental observation that bromination of **II** occurs at the 2,7-positions selectively.

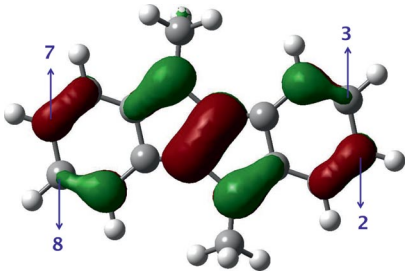

Figure 4. Plots (isovalue = 0.04 au) of the HOMO of **II** calculated at the B3LYP/6-311G (d,P) level.

Furthermore, to gain more insight into the molecular orbital properties of 2,7-DPPIIDPP, quantum-chemical calculations were performed with the Gaussian09 suite, employing the B3LYP and TD-B3LYP density functionals in combination with the 6-311G (d,p) basis set. Again, all the side-chain substituents were replaced by methyl groups for simplicity. The computational details are provided in the Supporting Information. The optimized geometry of 2,7-DPPIIDPP is depicted in Figure 5. As can be seen from the top-view graph in Figure 5, this molecule has a fairly planar structure, which is believed to be the primary factor that renders this material crystalline.

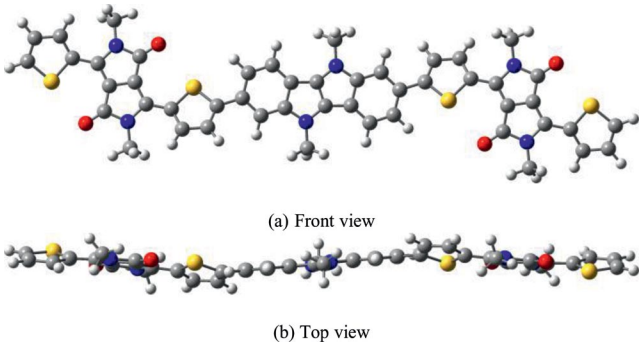

Figure 5. (a) Front view and (b) top view of the optimized geometry of 2,7-DPPIIDPP at the B3LYP/6-311G(d,p) level, with solvation in $CHCl_3$. Yellow: sulfur; blue: nitrogen; gray: carbon; light-gray: hydrogen.

The calculated HOMO/LUMO energy, excitation energy, oscillator strength, and configuration of the excited state are summarized in Table 2. The most probable vertical excitations are calculated to be 673 and 424 nm, which are both

more redshifted than their experimental λ_{max} (625 and 401 nm). Although there are variations in the absolute values, the calculated estimates should still be representative of the experimental data. The frontier orbitals of the model compound 2,7-DPPIIDPP are illustrated in Figure 6. The electron density of the HOMO is homogeneously distributed along the molecular backbone, except that the outmost thiophenes have lower electron density. However, the electron density of the LUMO is mainly localized in the DPP acceptor. Such an electronic redistribution would normally result in a pronounced intramolecular charge separation between donor and acceptor after excitation. To gain further understanding of these electronic transitions, electron density difference maps (EDDMs) were constructed.[11] The electronic transitions can therefore be visualized through EDDMs. Red indicates a decrease in charge density, while green indicates an increase. As shown in Figure 7, the lowest energy singlet electronic transition (λ_{max} = 673 nm) of 2,7-DPPIIDPP is mainly a result of ICT from **II** to DPP units and the π–π* transition within the DPP unit has only a minor contribution. Another electronic transition at λ_{max} = 424 nm shows localized π–π* transitions independently on the DPP and **II** groups, respectively.

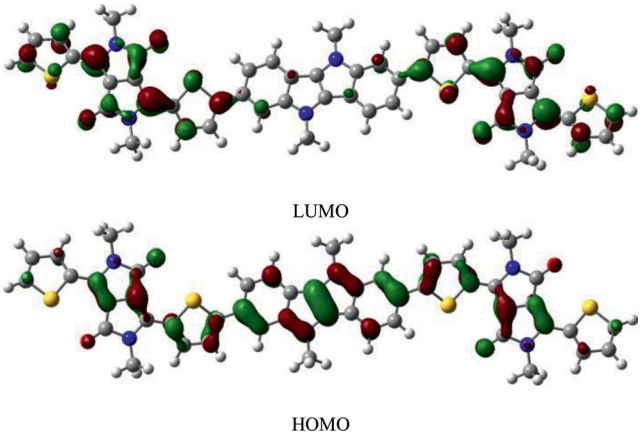

Figure 6. Plots (isovalue = 0.03 au) of frontier orbitals of 2,7-DPPIIDPP calculated at the B3LYP/6-311G (d,P) level in chloroform.

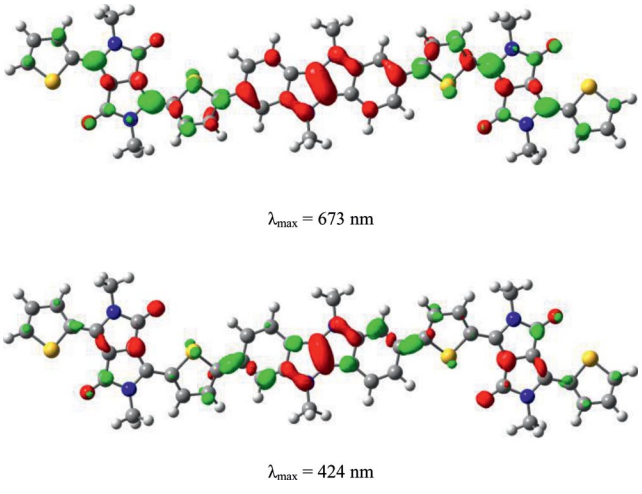

Figure 7. Electron density difference maps (EDDMs) of selected singlet electronic transitions of 2,7-DPPIIDPP at 673 and 424 nm. Red indicates a decrease in charge density, while green indicates an increase. All EDDMS were plotted with isovalue 0.0012 au.

Photovoltaic Characteristics

Bulk heterojunction photovoltaic cells were fabricated on the basis of indium tin oxide (ITO)/poly-3,4-ethylenedioxythiophene (PEDOT):poly-styrenesulfonate (PSS)/2,7-DPPIIDPP:$PC_{71}BM$/Ca/Al device configuration and their performances were measured under a simulated AM1.5G illumination of 100 mW cm^{-2}. The current density-voltage characteristics of the devices are illustrated in Figure 8. The optimized conditions for the devices are summarized in Table 3. The device based on a 2,7-DPPIIDPP/$PC_{71}BM$ blend (optimal ratio, 1:1 wt.-%) showed a V_{oc} of 0.78 V, a J_{sc} of 4.54 mA/cm^2, a FF of 38.0%, and a power conversion efficiency (PCE) of 1.35%. More importantly, the device efficiency could be enhanced significantly by thermal annealing of the active layers. After thermal annealing at 150 °C for 7 min, the device exhibited a V_{oc} of 0.72 V, a J_{sc} of 6.88 mA/cm^2, a FF of 49.6%, and a higher PCE of 2.45%. The J_{sc} value calculated from the integral of the external quantum efficiency (EQE) curve with an AM1.5G reference spectrum was 6.85 mA/cm^2, which is consistent with the value obtained from the *J*-*V* measurement (Figure 8). It should be noted that there was almost no response between 800 to 900 nm in the EQE spectrum, although the absorption of 2,7-DPPIIDPP actually spans from 300 to 900 nm. It can be reasonably deduced that the presence of $PC_{71}BM$ may reduce the degree of aggregation of 2,7-DPPIIDPP in the solid state. Furthermore, the 2,7-DPPI-

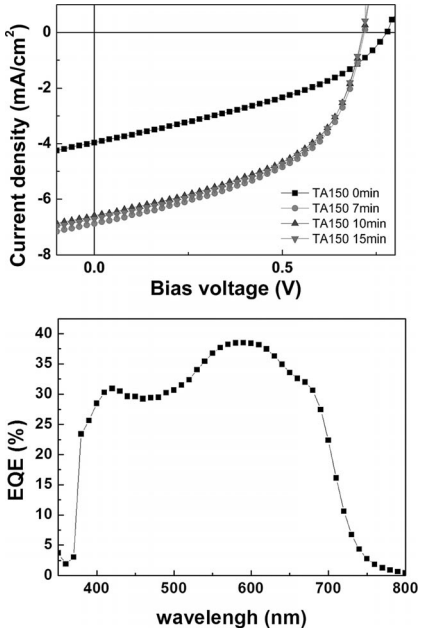

Figure 8. Current density-voltage characteristics (top) and EQE spectrum (bottom) of ITO/PEDOT:PSS/2,7-DPPIIDPP:$PC_{71}BM$/Ca/Al devices under illumination by AM 1.5G at 100 mW cm^{-2}.

IDPP content was reduced when $PC_{71}BM$ was included in a 1:1 ratio. Therefore, diminution of absorption intensity in the longer wavelengths for 2,7-DPPIIDPP in the blending systems is rational and even expected. Subsequently, increasing the thermal-annealing time to 10 or 15 min does not further change the efficiency (Table 3). To investigate the influence of thermal annealing on the active layer, temperature-dependent UV/Vis absorption measurements were conducted. After thermal annealing at 150 °C, the 2,7-DPPIIDPP:$PC_{71}BM$ blend film exhibited a substantial enhancement of the absorption intensity due to the thermal-driven molecular assembly leading to stronger interchain interactions (Figure 9). This improved device performance may be attributed to better charge transporting properties associated with higher molecular ordering of 2,7-DPPI-IDPP.

Table 3. Device characteristics with 2,7-DPPIIDPP/$PC_{71}BM$ (1:1 w/w).

Conditions	V_{oc} [V]	J_{sc} [mA/cm^2]	FF [%]	PCE [%]
No TA[a]	0.78	–4.54	38.0	1.35
TA 150 °C 7 min	0.72	–6.88	49.6	2.45
TA 150 °C 10 min	0.70	–6.70	50.3	2.36
TA 150 °C 15 min	0.72	–6.72	49.4	2.39

[a] TA: thermal annealing.

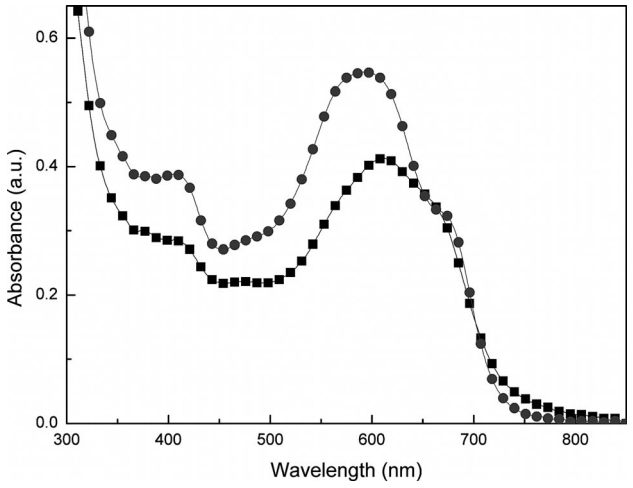

Figure 9. Absorption spectra of 2,7-DPPIIDPP/$PC_{71}BM$ (1:1 wt.-%) before (squares) and after (circles) thermal annealing at 150 °C.

Conclusions

We have developed a new synthetic route leading to indolo[3,2-*b*]indole derivatives. We discovered that the 2,7-positions of these fused ring systems have stronger electron-density and thus nucleophilicity than the 3,8-positions. Functionalization at the 2,7-positions of **II** not only preserve the phenylene units in the *para*-conjugation but also render stronger electron-donating strength. A conjugated A–D–A small molecule, 2,7-DPPIIDPP, was therefore obtained by the Suzuki coupling reaction. Due to its high coplanarity and strong donor-acceptor interaction through the 2,7-linkage, this material exhibited crystalline nature and broad UV/Vis absorption. The molecular orbital properties and electronic transitions of 2,7-DPPIIDPP have been elucidated in detail by TD-DFT calculations. Solution-processed small-molecule bulk heterojunction photovoltaic cells based on ITO/PEDOT:PSS/2,7-DPPIIDPP:$PC_{71}BM$ (1:1, w/w)/Ca/Al were fabricated and characterized. The device thermally annealed at 150 °C exhibited a V_{oc} of 0.72 V, a J_{sc} of 6.88 mA/cm^2, and a FF of 49.6%, leading to a PCE of 2.45%. This value is promising for small molecule-based solution processed BHJ solar cells. We anticipate that the 2,7-diboronic ester-indolo[3,2-*b*]-indole monomer presented in this research will emerge as an attractive building block for the construction of a series of new conjugated polymers and small molecules based on 2,7-substituted **II**. Follow-up research is underway in our laboratory.

Experimental Section

General Measurement and Characterization: All chemicals were obtained from commercial sources and used as received unless otherwise specified. Tetrahydrofuran (THF) was dried by distillation from sodium benzophenone ketyl. Anhydrous toluene and dichloromethane were obtained from a SD-300 solvent purification system (AsiaWong Enterprise). Fourier transform infrared (FTIR) spectra were recorded with a Perkin–Elmer One instrument. NMR measurements were recorded with a Varian Unity-300 spectrometer (^{1}H, 300 MHz; ^{13}C, 75 MHz). Chemical shifts (δ) are reported in ppm with respect to Me_4Si (δ = 0 ppm) for ^{13}C and ^{1}H NMR spectroscopy. Coupling constants (J) are given in Hz. ^{13}C NMR was proton broadband-decoupled. Multiplicities of peaks are denoted by the following abbreviations: s, singlet; d, doublet; t, triplet; m, multiplet; br, broad. Thermogravimetric analysis (TGA) was recorded with a PerkinElmer Pyris analyzer under nitrogen atmosphere at a heating rate of 10 °C/min. Absorption spectra were collected with a HP8453 UV/Vis spectrophotometer. The molecular weight of polymers was determined by gel permeation chromatography with a Viscotek VE2001GPC instrument, polystyrene was used as the internal standard, and THF as the eluent. Electrochemical cyclic voltammetry (CV) was conducted with a CH Instruments Model 611D analyzer. A carbon glass coated with a thin film was used as the working electrode and a Ag/Ag^+ electrode as the reference electrode; 0.1 M tetrabutylammonium hexafluorophosphate in acetonitrile was used as the electrolyte. CV curves were calibrated by using ferrocene as the standard, the oxidation potential of which was set at –4.8 eV with respect to zero vacuum level. The HOMO energy levels were obtained from the equation HOMO = $-(E_{ox}^{onset} - E_{(ferrocene)}^{onset} + 4.8)$ eV. The LUMO levels were obtained from the equation LUMO = $-(E_{red}^{onset} - E_{(ferrocene)}^{onset} + 4.8)$ eV.

4,4′-(Ethyne-1,2-diyl)bis(3-nitroaniline) (4): To a mixture of **3** (7.44 g, 45.88 mmol), 4-iodo-3-nitroaniline (10.81 g, 40.94 mmol), degassed triethylamine (10 mL), and degassed THF (100 mL), was added [$PdCl_2(PPh_3)_2$] (0.72 g, 1.03 mmol) and copper iodide (0.39 g, 2.05 mmol). The reaction mixture was stirred for 2 h at room temperature under a nitrogen atmosphere. The solvent was removed and the residue was then purified by column chromatography on silica gel (hexane/THF, 5:1 v/v) to furnish **4** (10.8 g, 88%) as a purple solid. ^{1}H NMR ([D$_6$]DMSO, 300 MHz): δ = 7.39 (d, J = 8.4 Hz, 2 H), 7.27 (d, J = 2.1 Hz, 2 H), 6.91 (dd, J = 2.3, 8.6 Hz,

2 H), 6.28 (br., 4 H) ppm. ^{13}C NMR ([D$_6$]DMSO, 75 MHz): δ = 150.0, 135.5, 132.2, 118.5, 108.8, 104.9, 89.5 ppm. HRMS (FAB): calcd. for $C_{14}H_{10}N_4O_4$ $[M]^{+\cdot}$ 298.0702; found 298.0708.

1,2-Bis(4-bromo-2-nitrophenyl)acetylene (5): To a solution of **4** (3.30 g, 11.06 mmol) in CH_3CN (50 mL) and sulfolane (25 mL) was added boron trifluoride–diethyl ether (d = 1.12 g/mL, 98+%, 5.6 mL, 43.31 mmol) at –30 °C and stirring was continued at this temperature for 10 min. *tert*-Butyl nitrite (d = 0.86 g/mol, 90%, 7.4 mL, 55.54 mmol) was then introduced and the mixture was gradually warmed to room temperature, stirred for 30 min, and charged with diethyl ether (100 mL). The formed salt was collected and mixed with copper(II) bromide and DMSO (40 mL). The mixture was stirred at room temperature for 2 h (***Caution:*** this reaction is exothermic and generates a significant amount of nitrogen gas) and then poured into water. The resultant precipitate was collected and purified by column chromatography on silica gel (hexane/CH_2Cl_2, 5:1 v/v) to afford **5** (1.88 g, 40%) as a yellow solid. IR (KBr): $\tilde{\nu}$ = 3089, 2919, 2850, 1549, 1342, 1273, 1093, 890, 835, 760, 536 cm^{-1}. ^{1}H NMR ($CDCl_3$, 300 MHz): δ = 8.31 (d, J = 2.0 Hz, 2 H), 7.79 (dd, J = 2.0, 8.3 Hz, 2 H), 7.68 (d, J = 8.3 Hz, 2 H) ppm. ^{13}C NMR ($CDCl_3$, 75 MHz): δ = 136.4, 136.1, 128.3, 128.1, 123.5, 118.5, 116.7 ppm. HRMS (FAB): calcd. for $C_{14}H_6Br_2N_2O_4$ $[M]^{+\cdot}$ 423.8694; found 423.8699.

1,2-Bis(4-bromo-2-nitrophenyl)ethane-1,2-dione (6): To a solution of **5** (1.06 g, 2.49 mmol) in acetone (100 mL) and acetic acid (1 mL) was added $KMnO_4$ (0.87 g, 5.51 mmol). The mixture was heated to reflux for 2 h, poured into acetone (500 mL), and sonicated for 10 min. After removal of the MnO_2 precipitate by filtration, the filtrate was evaporated and the residue was purified by chromatography on silica gel (hexane/CH_2Cl_2, 5:1 v/v) to afford **6** (1.13 g, 99%) as a yellow solid. IR (KBr): $\tilde{\nu}$ = 3426, 3087, 2923, 2853, 1721, 1602, 1535, 1464, 1341, 1262, 1201, 1080, 968, 865, 823, 732, 548 cm^{-1}. ^{1}H NMR ($CDCl_3$, 300 MHz): δ = 8.41 (d, J = 1.5 Hz, 2 H), 8.01 (dd, J = 1.8, 8.1 Hz, 2 H), 7.53 (d, J = 8.1 Hz, 2 H) ppm. HRMS (FAB): calcd. for $C_{14}H_6Br_2N_2O_6$ $[M]^{+\cdot}$ 455.8593; found 455.8585.

2,7-Dibromo-5,10-dihydroindolo[3,2-*b*]indole (7): A mixture of **6** (0.72 g, 1.75 mmol) and acetic acid (25 mL) was heated to 80 °C and stirred vigorously for 5 min. Tin(II) chloride dihydrate (3.55 g, 15.73 mmol) and $HCl_{(aq)}$ (1N, 3 mL) were introduced and the mixture was stirred for 5 h at 80 °C. The reaction proceeded through stages characterized by a yellow suspension, a red solution, and finally a yellow suspension. The resulting precipitate was collected and washed with acetic acid and methanol to give **7** (0.21 g, 37%) as a yellow solid. IR (KBr): $\tilde{\nu}$ = 3647, 3414, 2956, 2921, 2852, 1646, 1442, 1402, 1363, 1313, 1252, 1161, 1049, 928, 849, 798 cm^{-1}. ^{1}H NMR ([D$_6$]DMSO, 300 MHz): δ = 10.61 (br., 2 H), 7.77 (d, J = 8.3 Hz, 2 H), 7.77 (d, J = 1.8 Hz, 2 H), 7.27 (dd, J = 1.7, 8.5 Hz, 2 H) ppm. HRMS (EI): calcd. for $C_{14}H_8Br_2N_2$ $[M]^{+\cdot}$ 361.9054; found 361.9059.

2,7-Dibromo-5,10-bis(2-ethylhexyl)indolo[3,2-*b*]indole (8): A mixture of NaH (60%, 273 mg, 6.83 mmol), **7** (620 mg, 1.70 mmol), and THF (50 mL) was heated to 70 °C for 10 min and 2-ethylhexyl bromide (95%, d = 1.08 g/mL, 0.96 mL, 5.10 mmol) was then introduced. The reaction was continued at this temperature for 24 h. After cooling to room temperature, the mixture was poured into water, extracted with diethyl ether, evaporated, and purified by column chromatography to furnish **8** (632 mg, 63%) as a white solid. ^{1}H NMR ($CDCl_3$, 300 MHz): δ = 7.61 (d, J = 8.4 Hz, 2 H), 7.54 (s, 2 H), 7.25 (br., 2 H), 4.20 (br., 4 H), 2.07 (br., 2 H), 0.81–1.38 (m, 28 H) ppm. ^{13}C NMR ($CDCl_3$, 75 MHz): δ = 141.8, 126.3, 121.5, 119.0, 115.5, 113.3, 113.2, 49.9, 40.4, 31.0, 28.8, 24.4, 23.2, 14.2, 11.2 ppm. HRMS (EI): calcd. for $C_{30}H_{40}Br_2N_2$ $[M]^{+\cdot}$ 586.1558; found 586.1550.

5,10-Bis(2-ethylhexyl)-2,7-bis(4,4,5,5-tetramethyl-1,3,2-dioxaborolan-2-yl)indolo[3,2-*b*]indole (9): A mixture of **8** (500 mg, 0.85 mmol), bis(pinacolato)diborane (518 mg, 2.04 mmol), [$PdCl_2$(dppf)] (16 mg, 0.02 mmol), potassium acetate (500 mg, 5.09 mmol), and DMF (20 mL; deoxygenated by a freeze-pump-thaw process) was heated at 140 °C for 2 d. After cooling to room temperature, the reaction mixture was poured into water and extracted with CH_2Cl_2. The collected organic layer was dried under vacuum. The residue was purified by column chromatography on silica gel (hexane/CH_2Cl_2, 5:1 v/v) and then recrystallized from ethanol to give **9** (240 mg, 41%) as light-olivine crystals. ^{1}H NMR ($CDCl_3$, 300 MHz): δ = 7.93 (s, 2 H), 7.84 (d, J = 8.1 Hz, 2 H), 7.59–7.62 (m, 2 H), 4.41 (br., 4 H), 2.17 (br., 2 H), 1.19–1.57 (m, 40 H), 0.81–0.89 (m, 12 H) ppm. ^{13}C NMR ($CDCl_3$, 75 MHz): δ = 141.0, 127.4, 123.9, 117.4, 116.7, 116.2, 83.6, 49.4, 40.3, 30.6, 28.7, 24.9, 24.2, 23.0, 14.1, 11.0 ppm. HRMS (EI): calcd. for $C_{42}H_{64}B_2N_2O_4$ $[M]^{+\cdot}$ 682.5052; found 682.5054.

2,7-DPPIIDPP: A mixture of **12** (60 mg, 0.09 mmol), **9** (106.1 mg, 0.18 mmol), potassium carbonate (91.7 mg, 0.66 mmol), Aliquat 336 (15.2 mg, 0.04 mmol), [$Pd(PPh_3)_4$] (2.0 mg, 0.002 mmol), toluene (5 mL), and water (1 mL) was added to a sealed tube filled with nitrogen. The mixture was heated at 110 °C for 2 d, then cooled to room temperature, poured into water, and extracted with CH_2Cl_2. The organic layer was mixed with Pd-thio gel and Pd-TAAcOH (Silicycle Inc.) to remove any residual metal. After filtration and removal of the solvent, the residue was recrystallized from ethanol/THF to give 2,7-DPPIIDPP (30 mg, 23%). ^{1}H NMR ($CDCl_3$, 300 MHz): δ = 9.10 (d, J = 3.9 Hz, 2 H), 8.88 (d, J = 2.7 Hz, 2 H), 7.84 (d, J = 8.1 Hz, 2 H), 7.71 (s, 2 H), 7.60–7.62 (m, 2 H), 7.51–7.56 (m, 4 H), 7.29 (s, 2 H), 4.39–4.42 (m, 4 H), 4.05–4.13 (m, 8 H), 2.19 (br., 2 H), 1.99 (br., 2 H), 1.89 (br., 2 H), 1.26–1.49 (m, 48 H), 0.83–0.98 (m, 36 H) ppm. ^{13}C NMR ($CDCl_3$, 75 MHz): δ = 162.1, 161.8, 152.2, 141.8, 140.8, 139.5, 137.9, 135.1, 130.4, 130.3, 128.6, 128.1, 128.0, 127.2, 123.9, 118.7, 117.2, 114.5, 108.4, 107.7, 107.7, 49.8, 46.2, 40.7, 39.5, 39.3, 31.1, 30.6, 30.5, 29.0, 28.7, 28.6, 24.5, 23.9, 23.8, 23.4, 23.3, 23.2, 14.3, 14.3, 14.2, 11.2, 10.9, 10.8 ppm. HRMS (FAB): calcd. for $C_{90}H_{118}N_6O_4S_4$ $[M]^{+\cdot}$ 1474.8097; found 1474.8088.

Device Fabrication: Indium tin oxide (ITO)-coated glass substrate was ultrasonically washed with detergent, deionized water, acetone, and 2-propanol sequentially (15 min each) and then cleaned under UV/ozone for another 15 min. PEDOT:PSS (Clevios PVP AI-4083) was filtered and spin-coated on the cleaned ITO-coated glass at 2000 rpm for 40 s to produce a 30 nm interlayer, followed by baking at 170 °C under a nitrogen atmosphere for 15 min. 2,7-DPPIIDPP was then mixed with $PC_{71}BM$ in 1:1 weight ratio in chloroform (the concentration of 2,7-DPPIIDPP was kept at 6 mg/mL). The prepared solution was heated to 60 °C, stirred for 6 h, and filtered with a 0.45 μm Teflon® syringe filter. It was then spin-coated on top of the PEDOT:PSS interlayer at 1200 rpm. The resultant film was covered with a Petri dish to allow the solvent to slowly evaporate (solvent annealing) until the film dried and then baked at 150 °C for 7–15 min (thermal annealing). The top electrode was then prepared by sequential thermal evaporation of Ca (35 nm) and Al (100 nm) at reduced pressure (below 10^{-6} Torr) to furnish the BHJ solar-cell devices. All devices contained an active area of 0.04 cm^2 and the photovoltaic parameters were measured at room temperature under air atmosphere with a Xenon lamp coupled to an AM 1.5G solar filter (SAN-EIXES-301S solar simulator). *J-V* characteristics were recorded with a Keitheley 2400 Source Measurement Unit.

Supporting Information (see footnote on the first page of this article): Computational details, NMR spectra, cyclic voltammogram of 2,7-DPPIIDPP.

Acknowledgments

The authors thank the National Science Council of Taiwan and the "ATU Program" of the Ministry of Education, Taiwan, the Center for Interdisciplinary Science (CIS) of the National Chiao Tung University, Taiwan for financial support. The authors are also grateful to the National Center for High-performance Computing (NCHC) in Taiwan for computer time and facilities.

[1] a) G. Yu, J. Gao, J. C. Hummelen, F. Wudl, A. J. Heeger, *Science* **1995**, *270*, 1789–1791; b) B. C. Thompson, J. M. J. Fréchet, *Angew. Chem.* **2008**, *120*, 62; *Angew. Chem. Int. Ed.* **2008**, *47*, 58–77; c) S. Gunes, H. Neugebauer, N. S. Sariciftci, *Chem. Rev.* **2007**, *107*, 1324–1388; d) Y.-J. Cheng, S.-H. Yang, C.-S. Hsu, *Chem. Rev.* **2009**, *109*, 5868–5923; e) J. Chen, Y. Cao, *Acc. Chem. Res.* **2009**, *42*, 1709–1718; f) H. Zhou, L. Yang, W. You, *Macromolecules* **2012**, *45*, 607–632.

[2] a) J. Zhou, X. Wan, Y. Liu, Y. Zuo, Z. Li, G. He, G. Long, W. Ni, C. Li, X. Su, Y. Chen, *J. Am. Chem. Soc.* **2012**, *134*, 16345–16351; b) Z. Li, G. He, X. Wan, Y. Liu, J. Zhou, G. Long, Y. Zuo, M. Zhang, Y. Chen, *Adv. Energy Mater.* **2012**, *2*, 74–77; c) J. Zhou, X. Wan, Y. Liu, G. Long, F. Wang, Z. Li, Y. Zuo, C. Li, Y. Chen, *Chem. Mater.* **2011**, *23*, 4666–4668; d) B. Walker, C. Kim, T.-Q. Nguyen, *Chem. Mater.* **2011**, *23*, 470–482; e) A. Mishra, P. Bäuerle, *Angew. Chem.* **2012**, *124*, 2060; *Angew. Chem. Int. Ed.* **2012**, *51*, 2020–2067; f) B. Ma, C. H. Woo, Y. Miyamoto, J. M. J. Fréchet, *Chem. Mater.* **2009**, *21*, 1413–1417; g) O. P. Lee, A. T. Yiu, P. M. Beaujuge, C. H. Woo, T. W. Holcombe, J. E. Millstone, J. D. Douglas, M. S. Chen, J. M. J. Fréchet, *Adv. Mater.* **2011**, *23*, 5359–5363; h) J. J. Jasieniak, B. B. Y. Hsu, C. J. Takacs, G. C. Welch, G. C. Bazan, D. Moses, A. J. Heeger, *ACS Nano* **2012**, *6*, 8735–8745; i) Z. B. Henson, G. C. Welch, T. van der Poll, G. C. Bazan, *J. Am. Chem. Soc.* **2012**, *134*, 3766–3779; j) Y. Sun, G. C. Welch, W. L. Leong, C. J. Takacs, G. C. Bazan, A. J. Heeger, *Nature Mater.* **2012**, *11*, 44–48; k) Q. Shi, P. Cheng, Y. Li, X. Zhan, *Adv. Energy Mater.* **2012**, *2*, 63–67; l) Y. Lin, Y. Li, X. Zhan, *Chem. Soc. Rev.* **2012**, *41*, 4245–4272; m) Y. Lin, P. Cheng, Y. Liu, Q. Shi, W. Hu, Y. Li, X. Zhan, *Org. Electron.* **2012**, *13*, 673–680.

[3] a) J. Roncali, *Chem. Rev.* **1997**, *97*, 173–205; b) H. A. M. van Mullekom, J. A. J. M. Vekemans, E. E. Havinga, E. W. Meijer, *Mater. Sci. Eng.* **2001**, *32*, 1–40; c) A. Ajayaghosh, *Chem. Soc. Rev.* **2003**, *32*, 181–191.

[4] a) N. Blouin, A. Michaud, D. Gendron, S. Wakim, E. Blair, R. Neagu-Plesu, M. Belletête, G. Durocher, Y. Tao, M. Leclerc, *J. Am. Chem. Soc.* **2008**, *130*, 732–742; b) Y.-J. Cheng, J.-S. Wu, P.-I. Shih, C.-Y. Chang, P.-C. Jwo, W.-S. Kao, C.-S. Hsu, *Chem. Mater.* **2011**, *23*, 2361–2369; c) J.-S. Wu, Y.-J. Cheng, T.-Y. Lin, C.-Y. Chang, P.-I. Shin, C.-S. Hsu, *Adv. Funct. Mater.* **2012**, *22*, 1711–1722; d) Y.-J. Cheng, Y.-J. Ho, C.-H. Chen, W.-S. Kao, C.-E. Wu, S.-L. Hsu, C.-S. Hsu, *Macromolecules* **2012**, *45*, 2690–2698.

[5] a) E. Zhou, S. Yamakawa, Y. Zhang, K. Tajima, C. Yang, K. Hashimoto, *J. Mater. Chem.* **2009**, *19*, 7730–7737; b) E. Zhou, J. Cong, K. Tajima, K. Hashimoto, *Chem. Mater.* **2010**, *22*, 4890–4895; c) Y. Xia, X. Su, Z. He, X. Ren, H. Wu, Y. Cao, D. Fan, *Macromol. Rapid Commun.* **2010**, *31*, 1287–1292; d) C. Yang, B. Li, J. Tong, Y. Xia, *Polym. Sci., Ser. A* **2011**, *53*, 469–479; e) H. J. Park, Y. Lee, J. W. Jo, W. H. Jo, *Polym. Chem.* **2012**, *3*, 2928–2932; f) J. Lu, F. Liang, N. Drolet, J. Ding, Y. Tao, R. Movileanu, *Chem. Commun.* **2008**, 5315–5317.

[6] T. Lei, Y. Cao, X. Zhou, Y. Peng, J. Bian, J. Pei, *Chem. Mater.* **2012**, *24*, 1762–1770.

[7] a) S. Qu, H. Tian, *Chem. Commun.* **2012**, *48*, 3039–3051; b) W. Li, W. S. C. Roelofs, M. M. Wienk, R. A. J. Janssen, *J. Am. Chem. Soc.* **2012**, *134*, 13787–13795; c) L. Dou, J. You, J. Yang, C.-C. Chen, Y. He, S. Murase, T. Moriarty, K. Emery, G. Li, Y. Yang, *Nat. Photonics* **2012**, *6*, 180–185.

[8] S. Bartoli, A. Cipollone, A. Squarcia, A. Madami, D. Fattori, *Synthesis* **2009**, 1305–1308.

[9] a) Y. Jin, K. Kim, S. Song, J. Kim, J. Kim, S. H. Park, K. Lee, H. Suh, *Bull. Korean Chem. Soc.* **2006**, *27*, 1043–1047; b) M. M. Murray, P. Kaszynski, D. A. Kaisaki, W. Chang, D. A. Dougherty, *J. Am. Chem. Soc.* **1994**, *116*, 8152–8161.

[10] a) K. Fukui, *Science* **1982**, *218*, 747–754; b) K. Fukui, T. Yonezawa, H. J. Shingu, *Chem. Phys.* **1952**, *20*, 722–725.

[11] N. M. O'Boyle, A. L. Tenderholt, K. M. Langner, *J. Comput. Chem.* **2008**, *29*, 839–845.

Received: March 26, 2013
Published Online: July 1, 2013

